Electronic Supplementary Material (ESI) for Physical Chemistry Chemical Physics.

ELECTRONIC SUPPORTING INFORMATION

Understanding Receptor-Mediated Endocytosis of Elastic Nanoparticle Through Coarse Grained Molecular Dynamic Simulation

Zhiqiang Shen

Department of Mechanical Engineering, University of Connecticut, Storrs, CT 06269, USA.

Huilin Ye

Department of Mechanical Engineering, University of Connecticut, Storrs, CT 06269, USA.

Ying Li

Department of Mechanical Engineering and Institute of Materials Science, University of Connecticut, Storrs, CT 06269, USA.

E-mail: yingli@engr.uconn.edu

1. Calibration of mechanical properties for model membrane

The bending rigidity of the planar membrane can be extracted from the membrane fluctuation spectrum [1, 2]. According to the membrane profile function $h(x, y)$ of a planar membrane, its Fourier transform could be expressed as:

$$h(q) = \frac{l}{L}\Sigma_n h(\mathbf{r}) \exp(i\mathbf{q} \cdot \mathbf{r}) \tag{1}$$

where L is the lateral side length of the planar membrane. l is the membrane patch length, when we divide the membrane into small patches to capture profile function $h(x, y)$. $\mathbf{q} = \frac{2\pi}{L}(n_x, n_y)$ is the wave vector. q is the norm of wave vector. Based on the equipartition theorem, the power spectrum is given as [3, 4]:

$$< |h(q)|^2 >= \frac{k_B T}{l^2[\kappa q^4 + \Sigma q^2]} \tag{2}$$

where κ and Σ are the bending rigidity and membrane tension, respectively. Then, the bending rigidity of membrane can be obtained by fitting the measured fluctuation spectrum to Eq.2 [1, 3, 5, 6].

For this numerical study, we built a flat square membrane in the xy plane with 7200 lipids. The membrane is relaxed by $2 \times 10^4\tau$ time steps. The membrane lateral tension is maintained at zero. And temperature of membrane is controlled at $T = 1.1\epsilon/k_B$. Afterwards, the membrane is further relaxed with $1 \times 10^5\tau$ time steps for fluctuation analysis. To measure the out-of-plane fluctuation, the membrane is divided into a 32×32 grid. Therefore, the patch length $l = L/32$. The average vertical displacement of each patch is calculated to get $h(x, y)$. Then we calculate the values of fluctuation spectra by 2 dimensional Fourier transform in MATLAB. By fitting the numerical data to Eq.2, we can get the membrane bending rigidity $\kappa = 13.636k_{\mathrm{B}}T$, which is $\kappa = 15\epsilon$, if we convert the unit to ϵ. This bending rigidity of model membrane lies within the experimental range ($10 \sim 50k_{\mathrm{B}}T$) [7, 8].

The stretching modules of membrane K_{MEM} could be calculated by measuring the relation between membrane tension and its projected area as below [6, 9]:

$$\Sigma = K_{\mathrm{MEM}}[A - A_0]/A_0 \tag{3}$$

where A is the lipid area, which is defined as project in-plane area of each lipid molecule. A_0 is lipid area at zero surface tension. In our simulation, we measured relation between membrane tension and lipid area, as shown in Fig. S1.B. In addition, the lipid area at zero surface tension is $1.132\sigma^2$. Therefore, the stretching modulus of membrane is around $22\epsilon/\sigma^2$.

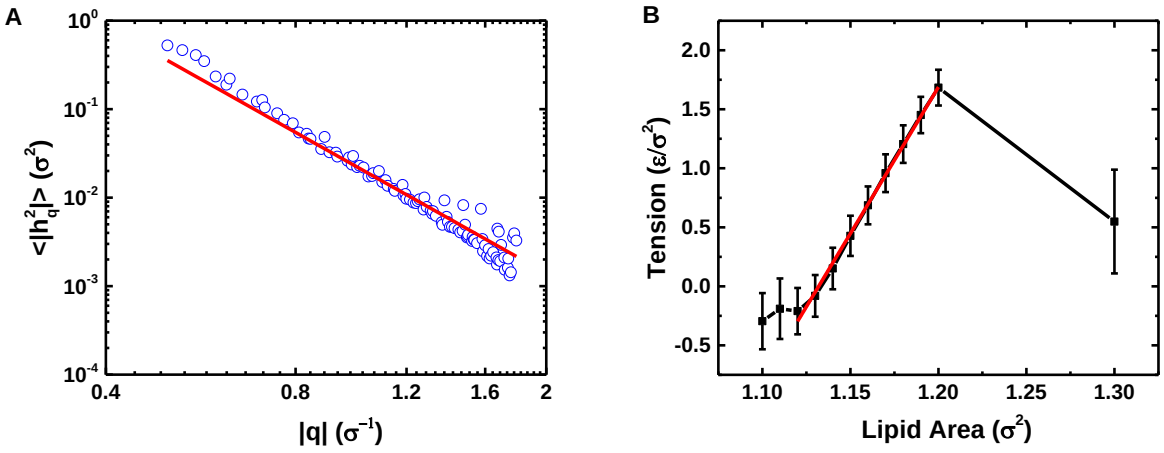

Figure S1: (A) Out-of-plane fluctuation spectrum of a planar membrane as a function of the wave number q. (B) Relation between membrane tension and lipid area.

2. Calibration of mechanical properties for elastic nanoparticles

To determine a suitable indenter velocity, we performed the indentation tests for NP ($R = 10\sigma$, $k_b = 100\epsilon$) with a series of indenter velocities (0.1, 0.05, 0.01, 0.005) σ/τ. The indenter radius is 15σ. The force applied by the indenter before the deformation of 6 σ is captured in Fig. S2, which is used to measured the stiffness of NP. We find that when the indenter velocity is larger than 0.01 σ/τ, the force- deformation curves are significantly affected by the indenter velocity. While, the force deformation curves are almost identical for indenter velocities of 0.01 and 0.005 σ/τ, indicating that the velocity of 0.01 σ/τ is small enough to avoid the potential indenter velocity effect. Therefore, we adopted the indenter velocity of 0.01 σ/τ to test the mechanical properties of elastic NPs.

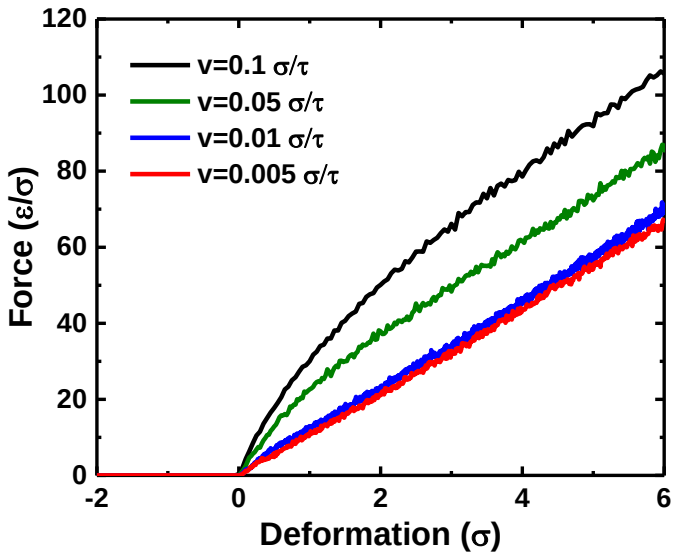

Figure S2: Force-deformation curves of NP ($R = 10\sigma$, $k_b = 100\epsilon$) with different indenter velocities.

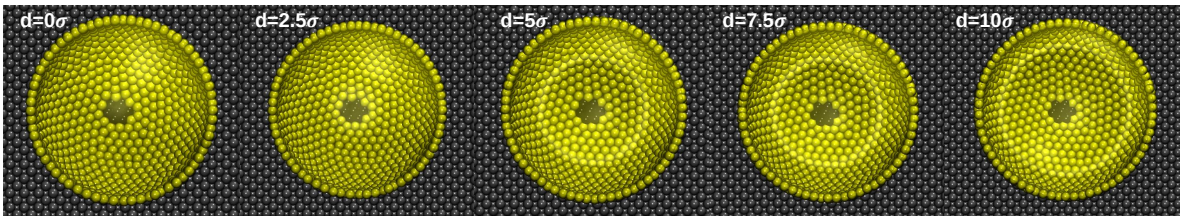

Figure S3: Top views of an elastic NP under different deformations. The corresponding side views are given in Fig.2.A of the main text. The radius of NP is $R = 10\sigma$ with bending rigidity $k_b = 1\epsilon$. The beads fixed on NP surface is colored in black. The top of NP is transparent to demonstrate its fixed bottom.

The phenomenal bending rigidity of each elastic NP in our simulation is obtained by the following equation [10]:

$$k_b^{\text{phen}} = \frac{\sqrt{3}k_{\text{stiff}}Rh}{48\sqrt{1-\nu^2}} \tag{4}$$

where k_{stiff} is the stiffness measured from nano-indentation tests. R and h are the radius and thickness of elastic NPs, respectively. Here we take $h = \sigma$ as the effective thickness of NP shell. ν is the Poisson ratio, which we take the value of 0.5 as that given in experiments [11]. As illustrated in Fig. S4, the phenomenal bending rigidity k_b^{phen} follows the same trend against bending rigidity k_b for elastic NPs with different radii.

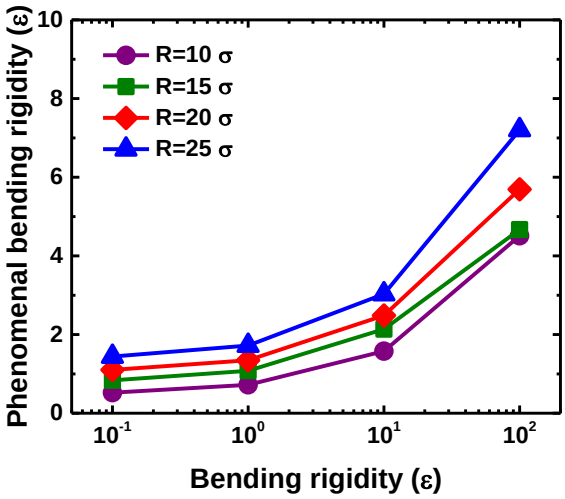

Figure S4: Relation between phenomenal bending rigidity k_b^{phen} and bending rigidity k_b of elastic nanoparticles.

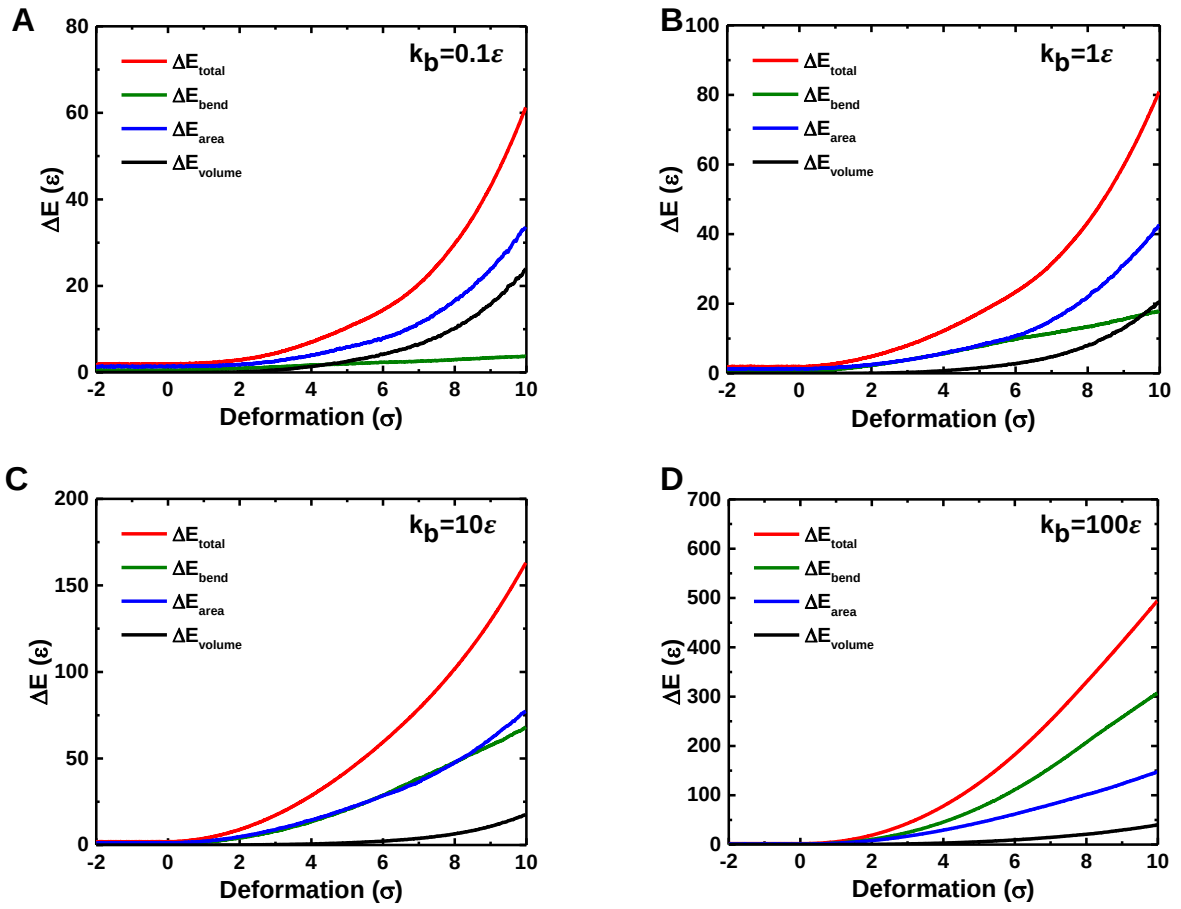

Figure S5: Energy change of elastic nanoparticles (NPs) during nano-indentation tests. (A-D) Energy changes of elastic NPs with bending rigidities of $k_b = 0.1, 1, 10, 100\epsilon$, respectively. The radius of NP is $R = 10\sigma$. ΔE_{volume} is the energy change associated with volume change. ΔE_{area} is the area energy change associated with area change. ΔE_{bend} is the bending energy change associated with the curvature change.

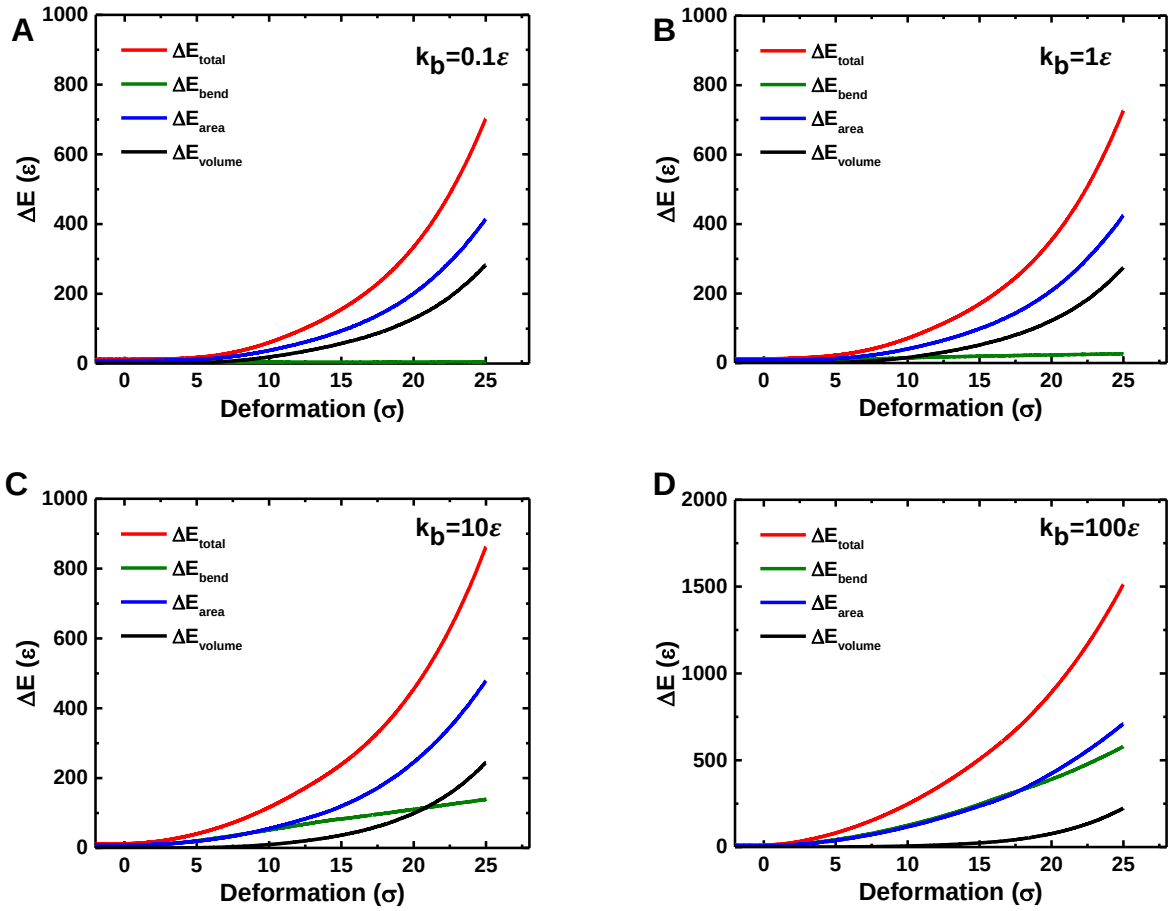

Figure S6: Energy change of elastic nanoparticles (NPs) during nano-indentation tests. (A-D) Energy changes of elastic NPs with bending rigidities of $k_b = 0.1, 1, 10, 100\epsilon$, respectively. The radius of NP is $R = 25\sigma$. ΔE_{volume} is the energy change associated with volume change. ΔE_{area} is the area energy change associated with area change. ΔE_{bend} is the bending energy change associated with the curvature change.

3. Membrane wrapping process of elastic nanoparticles

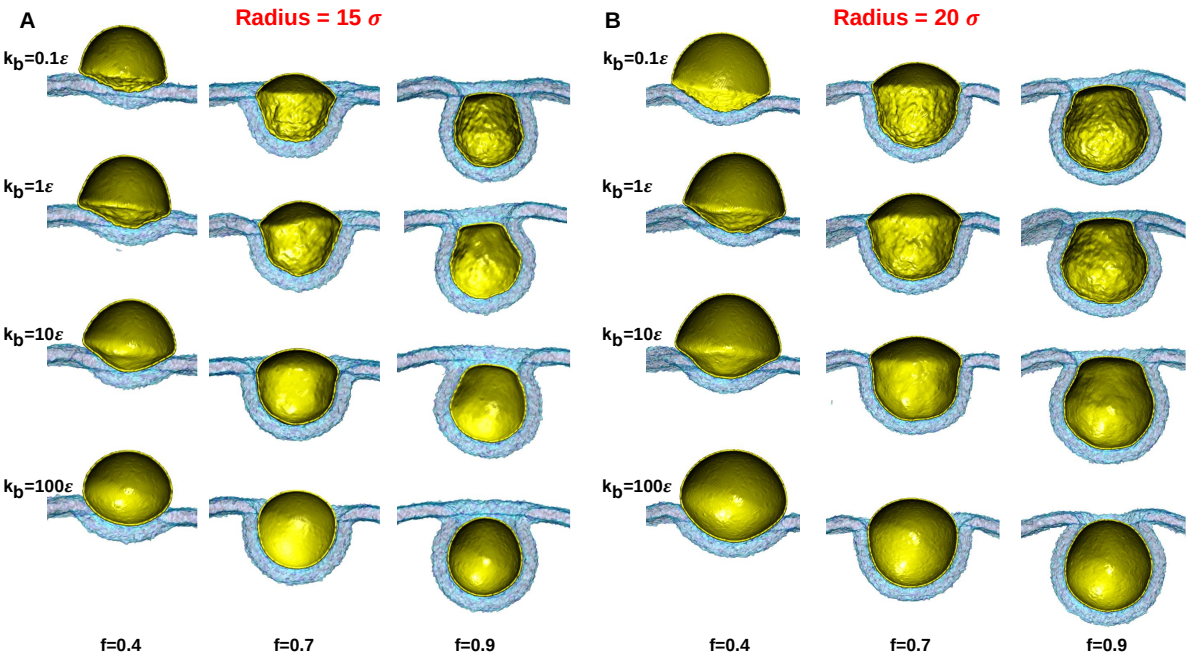

Figure S7: Configurations for the deformation of elastic NPs with different bending rigidities. (A) Comparisons of membrane and NP ($R = 15\sigma$) with bending rigidities $k_b = 0.1, 1.0, 10, 100\epsilon$ under wrapping ratios of $f = 0.4, 0.7$ and 0.9. (B) Comparisons of membrane and NP ($R = 20\sigma$) with bending rigidities $k_b = 0.1, 1.0, 10, 100\epsilon$ under wrapping ratios of $f = 0.4, 0.7$ and 0.9. The NP is colored in yellow. The membrane is colored with semi-transparent blue. The ligand is not shown on NP surface for clarity.

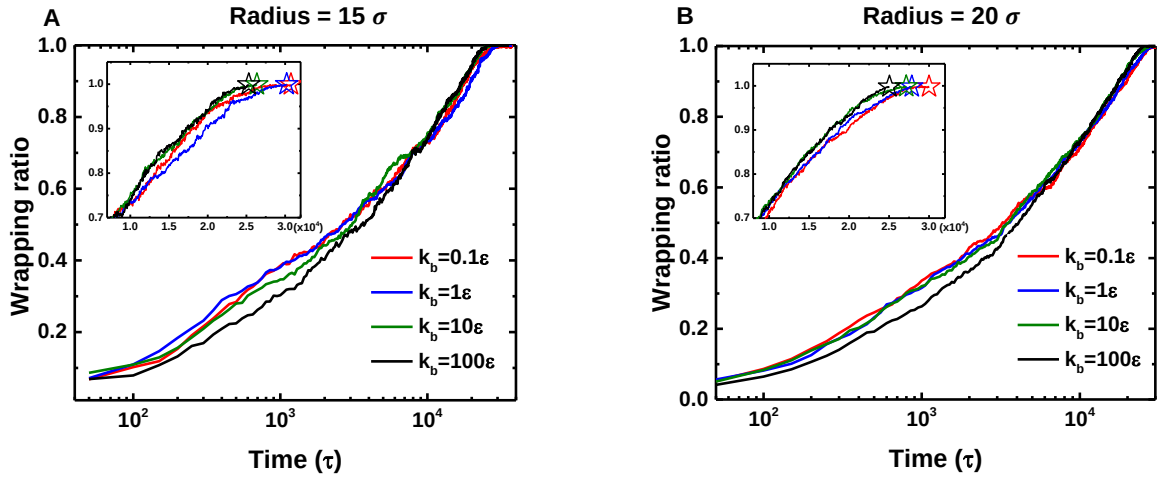

Figure S8: Comparison of wrapping ratio for elastic NPs with different bending rigidities. (A) Evolution of wrapping ratio for NP with radius $R = 15\sigma$. (B) Evolution of wrapping ratio for NP with radius $R = 20\sigma$. The insets are the wrapping ratio near the end of membrane wrapping process.

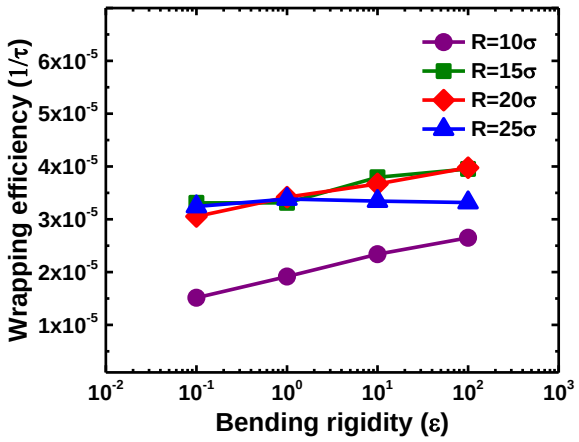

Figure S9: Comparison of wrapping efficiency of NPs with different bending rigidities and radii.

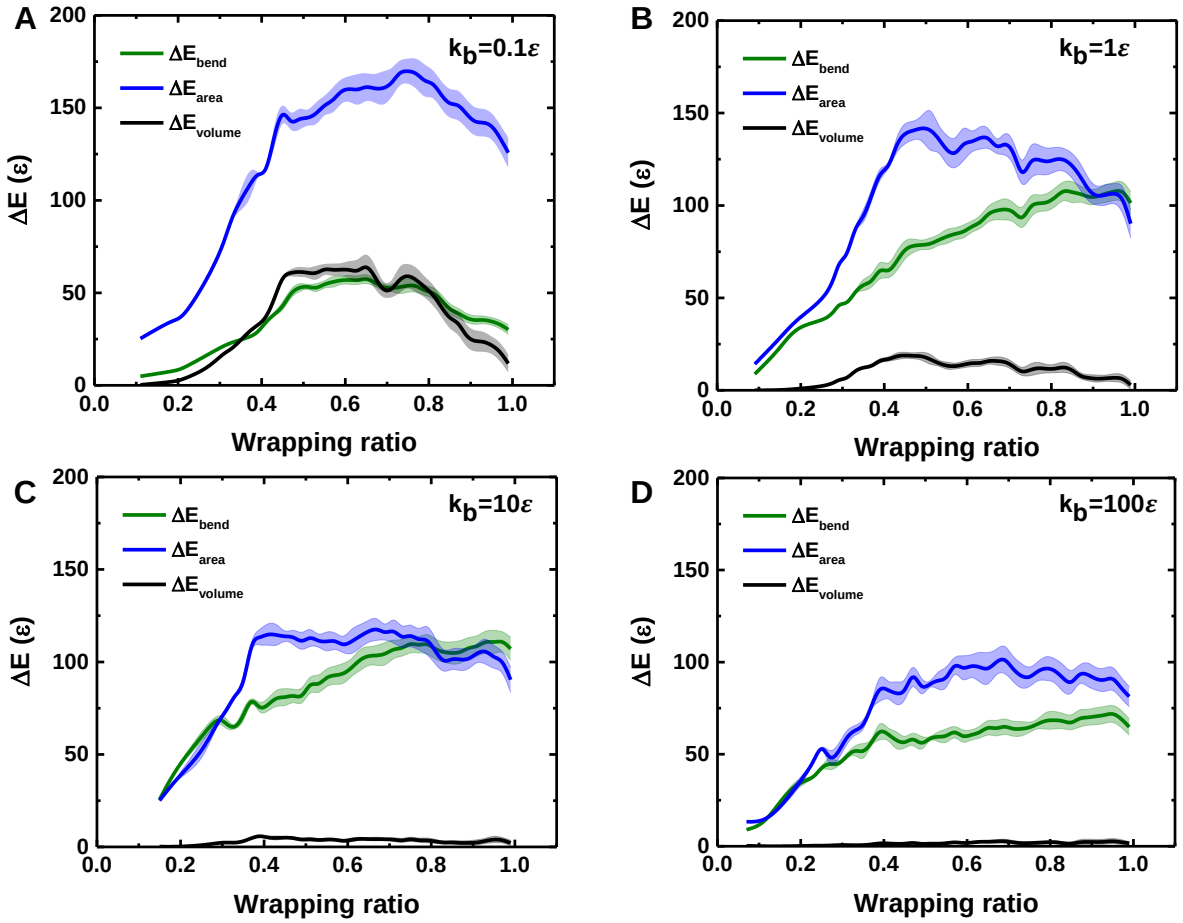

Figure S10: Energy change of elastic NPs during membrane wrapping process. (A-D) Energy changes of NPs with bending rigidities of $k_b = 0.1, 1, 10, 100\epsilon$. The radius of NP is $R = 10\sigma$. ΔE_{volume} is the energy change associated with volume change. ΔE_{area} is the area energy change associated with area change. ΔE_{bend} is the bending energy change associated with the curvature change.

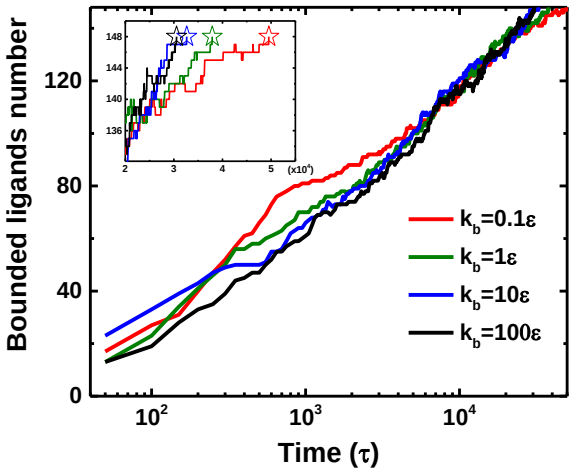

Figure S11: The evolution of bound ligands on NP surface during membrane wrapping process. The radius of NP is $R = 10\sigma$.

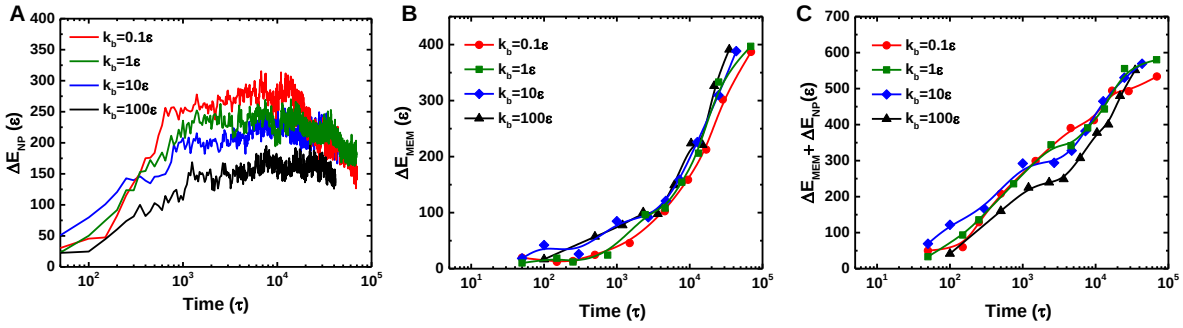

Figure S12: Evolution of energy change for elastic NPs with radius $R = 10\sigma$. (A) The evolution of energy change of NPs (ΔE_{NP}). (B) The evolution of energy change of membrane (ΔE_{MEM}) . (C) The evolution of total energy barrier ($\Delta E_{\mathrm{NP}} + \Delta E_{\mathrm{MEM}}$).

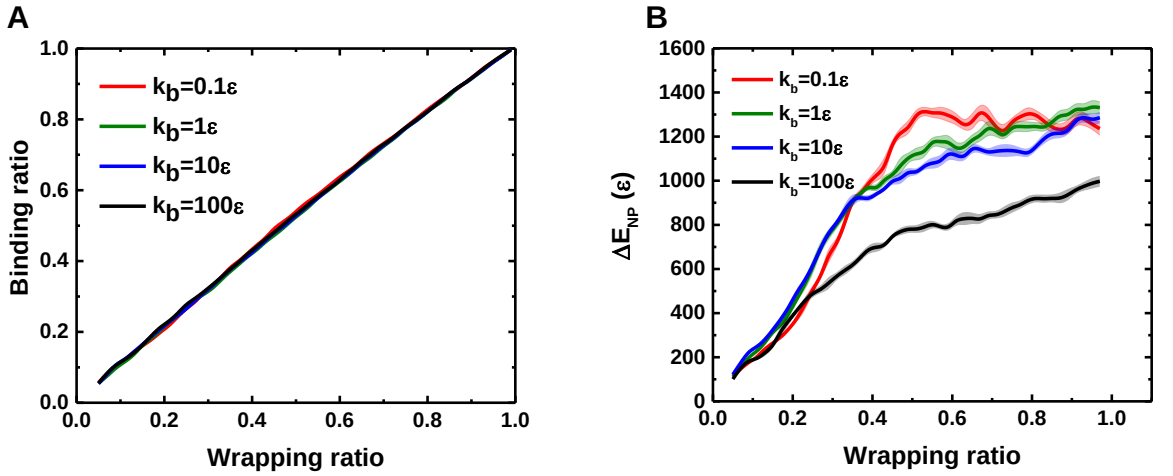

Figure S13: Ligand-receptor binding ratio and elastic energy change of NP with radius $R = 25\sigma$. (A) The relation between ligand-receptor binding ratio and membrane wrapping ratio. (B) The relation between elastic energy change of NPs and membrane wrapping ratio.

References

[1] Ira R Cooke and Markus Deserno. Solvent-free model for self-assembling fluid bilayer membranes: stabilization of the fluid phase based on broad attractive tail potentials. *The Journal of chemical physics*, 123(22):224710, 2005.

[2] David Boal and David H Boal. *Mechanics of the Cell*. Cambridge University Press, 2012.

[3] He Li and George Lykotrafitis. Two-component coarse-grained molecular-dynamics model for the human erythrocyte membrane. *Biophysical journal*, 102(1):75–84, 2012.

[4] Wolfgang Helfrich. Elastic properties of lipid bilayers: theory and possible experiments. *Zeitschrift für Naturforschung C*, 28(11-12):693–703, 1973.

[5] S-P Fu, Z Peng, H Yuan, R Kfoury, and Y-N Young. Lennard-jones type pair-potential method for coarse-grained lipid bilayer membrane simulations in lammps. *Computer Physics Communications*, 210:193–203, 2017.

[6] Rüdiger Goetz, Gerhard Gompper, and Reinhard Lipowsky. Mobility and elasticity of self-assembled membranes. *Physical Review Letters*, 82(1):221, 1999.

[7] W Rawicz, KC Olbrich, T McIntosh, D Needham, and E Evans. Effect of chain length and unsaturation on elasticity of lipid bilayers. *Biophysical journal*, 79(1):328–339, 2000.

[8] Rubèn Serral Gracià, Natalya Bezlyepkina, Roland L Knorr, Reinhard Lipowsky, and Rumiana Dimova. Effect of cholesterol on the rigidity of saturated and unsaturated membranes: fluctuation and electrodeformation analysis of giant vesicles. *Soft Matter*, 6(7):1472–1482, 2010.

[9] Julian C Shillcock and Reinhard Lipowsky. Equilibrium structure and lateral stress distribution of amphiphilic bilayers from dissipative particle dynamics simulations. *The Journal of chemical physics*, 117(10):5048–5061, 2002.

[10] N Delorme and A Fery. Direct method to study membrane rigidity of small vesicles based on atomic force microscope force spectroscopy. *Phys Rev E*, 74(3):030901, 2006.

[11] Yuki Takechi-Haraya, Yukihiro Goda, and Kumiko Sakai-Kato. Control of liposomal penetration into three-dimensional multicellular tumor spheroids by modulating liposomal membrane rigidity. *Mol Pharmaceutics*, 2017.